EUROPEAN JOURNAL OF COMPUTATIONAL MECHANICS, 2015
VOL. 24, NO. 6, 256–278
http://dx.doi.org/10.1080/17797179.2016.1181028

Taylor & Francis
Taylor & Francis Group

Study of geometric non-linear instability of 2D frame structures

Said Mamouri[a], Elhoucine Mourid[b] and Adnan Ibrahimbegovic[c]

[a]L_2ME UTM Bechar, Mechanical Engineering Department, Bechar, Algeria; [b]LMS UTM Bechar, Mechanical Engineering Department, Bechar, Algeria; [c]Sorbonne universités, Université de technologie de Compiègne, CNRS UMR7337 Laboratoire Roberval, Centre de Recherche Royallieu, Compiegne, France

ABSTRACT

In this work, we deal with the geometric instability problem of the two-dimensional (2D) elastic frame structures undergoing large overall motion. The geometrically exact beam model with total Lagrangian formulation is used to obtain the solution to non-linear instability problems with large pre-buckling displacements. We propose, in particular, a study of dynamic analysis that can deal with instability problems of this kind with no need for any load decrease. The dynamics approach provides a more realistic post-buckling behaviour for the case of snap-through or snap-back. The material damping is necessary when a classical time integration scheme like Newmark is used. The principal novelty in this work is to consider non-linear damping to avoid the vibration around the equilibrium point when a classical scheme as Newark is used. The efficiency of the damping model and methodology analysis are illustrated by a number of numerical simulations.

ARTICLE HISTORY
Received 24 June 2015
Accepted 18 April 2016

KEYWORDS
Geometric instability; post-buckling; dynamic; geometrically exact beam

1. Introduction

A number of recent researches have dealt with non-linear behaviour of the frame structure undergoing large displacements and rotations (e.g. Armentani, Cali, Cricrí, Caputoc, & Esposito, 2006; Ibrahimbegović, Shakourzadeh, Batoz, AI Mikdad, & Guo, 1996; Ibrahimbegović & Mamouri, 1999; Meek & Xue, 1996, 1998). This can lead to decreasing structure stiffness with the load increase, eventually reaching the instability points where the stiffness matrix becomes singular. Even in the neighbourhood of instability points we find that a small increase in loading leads to disproportional increase of computed response. It is important to be able to distinguish between two types of instability: by limit point or by bifurcation point (e.g. see Ibrahimbegovic, 2009), knowing that the numerical solution procedure is quite different (e.g. see Ibrahimbegović & Al Mikdad, 2000).

CONTACT Said Mamouri mamouri.said@mail.univ-bechar.dz

However, the singularity of the stiffness matrix at the limit point does not necessarily mean the collapse of structure. The structure may merely pass through a critical point or exhibit a snap-back behaviour, with the corresponding decrease in stiffness. In any such case, it is important to perform the post-buckling analysis, which requires not only to find the critical point but also to explore the post-critical regime.

Before the critical point, incremental technique combined with the Newton iterative procedure is typically used with static analysis. However, such an incremental load approach in the neighbourhood of the critical load can lead to divergence, due to singularity of the stiffness matrix. Moreover, any further increase in load after the limit point is prevented by instability.

Different numerical techniques to compute non-linear response are presented in Crisfield (Crisfield, 1991). For example, the displacement control method can be used to handle the snap-through, but it cannot be used for the snap-back behaviour. For this type of instability, we must use the arc-length method (Crisfield, 1991) which is the most robust and most efficient to trace the equilibrium path after the limit point. (Ibrahimbegović & Al Mikdad, 2000; Crisfield, 1991; Ibrahimbegovic, Knopf-Lenoir, Kucerova, & Villon, 2004).

If fact, all previous techniques used to trace the equilibrium path after the limit point are based upon the load decrease. It is interesting to analyse the behaviour of the structure if we continue this kind of exploration beyond the limit point, but without load decrease. Such a study was carried out in this work using a non-linear dynamics technique. For such analysis we use a slow loading rate, and place the response within the dynamics framework. The response can be computed by the implicit Newmark time integration scheme. This scheme is unconditionally stable for choice ($\beta = 1/4$ and $\gamma = 1/2$)for linear problems, whereas typically small time steps are needed in non-linear analysis to ensure the stability. In order to enhance the computational efficiency, the analysis is performed under quasi-static load control conditions until reaching the critical equilibrium point, and under non-linear dynamics, subsequently. The key point in transition from statics to dynamics pertains to keep a slow rate for load increase when tracing the load-deflection path in post-critical the regime. In order to recover the corresponding static solution response with such dynamic analysis, it is mandatory to introduce a damping to avoid this vibration. The novelty in this work is to consider non-linear damping avoiding the vibration around the equilibrium point.

However, this is not always enough, especially for stiff problems as demonstrated in (Bathe & Noh, 2012; Ibrahimbegović & Mamouri, 1999). In such a case, we need energy decaying schemes. The one employed herein is the Hilbert–Hughes–Taylor (HHT) scheme (Hilber, Hughes, & Taylor, 1977), or rather its generalisation HHT-α (e.g. see (Chung & Hulbert, 1993; Mamouri & Ibrahimbegovic, 2001)) that provides even a better compromise between the stability and accuracy requirements compared to the Newmark scheme. We can

also use more sophisticated energy-decaying schemes (e.g. (Ibrahimbegovic & Mamouri, 2002)) in order to ensure the stability.

Namely, various beam models formulations have been proposed for modelling the non-linear behaviour of the frame structures Meek and Xue (1996, 1998), Tan 1985, Belytschko and Hsieh (1973) or Bathe, Ramm, and Wilson (1976), have used the two-node element for Euler-Bernoulli beam model based upon the co-rotational formulation, which is considered as the simplest updated Lagrangian formulation (e.g. Ibrahimbegović et al., 1996). The second novelty concerns the use of the geometrically exact beam model in the proposed instability framework. In this work, we choose the geometrically exact beam developed by Ibrahimbegovic et al. (Ibrahimbegović, 1995; Ibrahimbegović & Frey, 1993), which can take into account the shear deformation. Furthermore, the choice of the total Lagrangian formulation in a fixed reference frame for describing the beam kinematics results with a constant mass matrix, which is the major advantage for the construction of time integration schemes. This formulation is more efficient than the previous ones using the rotated framed to simplify internal force computation, which remains limited to two nodes finite element.

The outline of this work is as follows. In the next section, we present the theoretical formulation of the geometrically exact beam model in the fully non-linear dynamics framework. In subsequent two sections we provide, respectively, the discrete approximation in space and in time, using the finite element method and the Newmark and HHT-α time stepping schemes. In section 4, we show the results of a number of illustrative examples. The last section gives several concluding remarks.

2. Dynamics of 2D beam undergoing large rotation

We consider a beam undergoing large rotation in 2D. The initial configuration is described by a vector position $\boldsymbol{\varphi}_0$ of point in neutral axis and the unit vector $\mathbf{t}_1^0$ normal to the beam cross section (see Ibrahimbegović & Frey, 1993):

$$\mathbf{t}_1^0 = \boldsymbol{\varphi}'_0 \tag{1}$$

where $(\bullet)' = \frac{d}{ds}(\bullet)$: denotes the partial derivative with respect to the s-coordinate, which is used to parameterise the beam initial configuration.

According to Reissner's hypothesis, the plane sections remain plane after deformation, but not necessarily perpendicular to the neutral axis of the beam (see Ibrahimbegović & Mamouri, 1999). Thus, the deformed configuration can be defined as:

$$\boldsymbol{\Phi}(s,t,\zeta) = \boldsymbol{\varphi}(s,t) + \zeta \mathbf{t}_2(s,t) \tag{2}$$

where $\boldsymbol{\varphi}$ is the position of point in the neutral axis, $\mathbf{t}_2$ is the unit vector attached to the cross section. In accordance with this basic kinematic hypothesis, the unit

vectors $\mathbf{t}_1$ and $\mathbf{t}_2$ are obtained by rotating their initial positions $\mathbf{t}_1^0$, $\mathbf{t}_2^0$. Thus, we define a two-dimensional (2D) rotation matrix $\mathbf{\Lambda}$ as:

$$\mathbf{t}_1 = \mathbf{\Lambda}\mathbf{t}_1^0, \mathbf{t}_2 = \mathbf{\Lambda}\mathbf{t}_2^0, \quad \text{with:} \quad \mathbf{\Lambda} = \begin{bmatrix} \cos\psi & -\sin\psi \\ \sin\psi & \cos\psi \end{bmatrix}$$

where ψ is the rotation angle around $\mathbf{t}_3$.
The corresponding generalised strain measure can then be written (see (Belytschko & Hsieh, 1973)):

$$\boldsymbol{\varepsilon} = \boldsymbol{\varphi}' - \mathbf{t}_1 \tag{3}$$

$$k = \psi' \tag{4}$$

where $\boldsymbol{\varepsilon}$ contains the axial and shear strains, and k is a bending strain. The stress resultants and couple are described in the deformed configuration with:

$$\mathbf{n} = n\mathbf{t}_1 + t\mathbf{t}_2 \tag{5}$$

$$\mathbf{m} = m\mathbf{t}_3 \tag{6}$$

where $n, m = \|\mathbf{m}\|$ are work-conjugate to $\boldsymbol{\varepsilon}, k$, respectively. We note that the stress resultants of this kind are the spatial objects acting in the deformed configuration, but parameterised by the coordinates set in the initial configuration. Thus, these are equivalent to the first Piola-Kirchhoff stress tensor.
The corresponding material description of stress resultants and their work-conjugate strain measures are obtained using the rotation matrix as:

$$\mathbf{\Sigma} = \mathbf{\Lambda}^{\mathrm{T}}\boldsymbol{\varepsilon}, K = k \tag{7}$$

$$\mathbf{N} = \mathbf{\Lambda}^{\mathrm{T}}\mathbf{n}, M = m \tag{8}$$

where,

$$\mathbf{N} = N\mathbf{t}_1 + T\mathbf{t}_2 \tag{9}$$

The linear elastic constitutes equations are chosen for stress resultants and couple with (see Belytschko & Hsieh, 1973):

The application of Hamilton's principle leads to the weak form of beam's equations of motion, which can be written as (see Ibrahimbegović & Mamouri, 1999):

$$\begin{pmatrix} N \\ T \end{pmatrix} = \mathbf{C}\begin{pmatrix} \Sigma \\ \Gamma \end{pmatrix}, \ \mathrm{M} = \mathrm{C}_{\mathrm{m}}k \tag{10}$$

$$\mathbf{C} = \begin{pmatrix} EA & 0 \\ 0 & GA \end{pmatrix}, \mathrm{C_m} = EI \tag{11}$$

where E is the young modulus, G is the shear modulus, A is the beam section, and I is the inertia of the section. The beam internal energy can be written in a quadratic form, using either material object:

$$\prod_{\text{int}} = \frac{1}{2}\int_0^l (\Sigma N + \Gamma T + KM)ds \tag{12}$$

or spatial objects:

$$\prod_{\text{int}} = \frac{1}{2}\int_0^l (\boldsymbol{\varepsilon}.\mathbf{n} + km)ds \tag{13}$$

where '•' denotes the scalar product of vectors.

$$\int_0^l (\delta\boldsymbol{\epsilon}.\delta\mathbf{n} + \delta k.m)ds + \int_0^1 (\delta\boldsymbol{\varphi}.A_\rho\ddot{\boldsymbol{\varphi}} + \delta\psi.I_\rho\ddot{\psi})ds - \delta\prod_{\text{ext}} = 0 \tag{14}$$

where $\ddot{\boldsymbol{\varphi}}, \ddot{\psi}$ are the acceleration components, $\delta\prod_{\text{ext}}$ is the virtual work of external forces and A_ρ, I_ρ are defined as: $A_\rho = \int \rho dA$ and $I_\rho = \int \rho\zeta^2 dA$
The virtual strains $\delta\boldsymbol{\varepsilon}, \delta k$ are obtained using the Lie derivative formalism (Marsden & Hughes, 1983). The principle is based on the pull-back of spatial objects in the material configuration, where their variations are computed, and the results are push-forward to the deformed configuration. Accordingly, the axial and shear virtual strains can be written as:

$$\delta\boldsymbol{\varepsilon} = \boldsymbol{\Lambda}\delta(\boldsymbol{\Lambda}^T\boldsymbol{\varepsilon}) = \delta\boldsymbol{\varphi}' - \mathbf{W}\boldsymbol{\varphi}'\delta\psi \tag{15}$$

where $\delta\boldsymbol{\varphi}', \delta\psi$ are, respectively, the virtual displacement and virtual rotation. Similarly, the virtual bending strain is computed by the Lie derivative, but in 2D this results in a very simple result, using the identity tensor for pull-back and push-forward due to planar nature of the problem:

$$\delta k = \delta\psi' \tag{16}$$

2.1. Finite element approximation

The weak form of equation of motion provides the most suitable form for finite element approximations. The mass matrix remains constant and non-linearity

is only in internal force expression. Contrary to co-rotational formulation (e.g. Belytschko & Hsieh, 1973; Bathe et al., 1976) that remains limited to two-node elements, the present formulation can be used for any number of nodes.

For a beam element with n_{en} node, the nodal interpolation of position vector and rotation are written as:

$$\boldsymbol{\varphi}(s) = \sum_{a=1}^{n_{\text{en}}} N_a(s)\boldsymbol{\varphi}_a \tag{17}$$

$$\psi(s) = \sum_{a=1}^{n_{\text{en}}} N_a(s)\psi_a \tag{18}$$

where $N_a(s)$ is the shape function for node a, which is chosen as Lagrange polynomial of order $(n_{\text{en}}-1)$. The same shape function is used for accelerations $\ddot{\boldsymbol{\varphi}}, \ddot{\psi}$ with corresponding nodal parameters. If the beam model mesh contains N_{el} elements, each with n_{en} nodes, the semi-discrete approximation of the weak form of the equation of motion can be written as:

$$\mathrm{A}\sum_{1}^{N_{\text{el}}}\left\{\sum_{a=1}^{n_{\text{en}}}\left\{\sum_{b=1}^{n_{\text{en}}}\begin{bmatrix}\mathbf{M}^e_{\text{ab}} & 0\\ 0 & \mathbf{H}^e_{\text{ab}}\end{bmatrix}\begin{pmatrix}\ddot{\boldsymbol{\varphi}}(t)\\ \ddot{\psi}(t)\end{pmatrix}+\begin{pmatrix}\mathbf{n}^e_a(t)\\ m^e_a(t)\end{pmatrix}-\begin{pmatrix}\bar{\mathbf{n}}^e_a(t)\\ \bar{m}^e_a(t)\end{pmatrix}\right\}\right\} \tag{19}$$

$\mathrm{A}\sum_{1}^{N_{\text{el}}}$ denotes the finite element assembly procedure. We denote with $\bar{\mathbf{n}}^e_a(t), \bar{m}^e_a(t)$ the external nodal forces and couple. Furthermore, $\mathbf{M}^e_{\text{ab}}, \mathbf{H}^e_{\text{ab}}$ are translational and rotational parts of the mass matrix with constant entries, described by:

$$\mathbf{M}^e_{ab} = \int_0^{l^e} N_a(s)\begin{bmatrix}A_\rho & 0\\ 0 & A_\rho\end{bmatrix}N_b(s)ds \tag{20}$$

$$\mathbf{H}^e_{ab} = \int_0^{l^e} N_a(s).I_\rho N_b(s)ds \tag{21}$$

Finally, the nodal internal forces are given as:

$$\mathbf{n}^e_a(t) = \int_0^{l^e} N'_a(s)\mathbf{n}ds \tag{22}$$

$$m^e_a(t) = \int_0^{l^e}\left\{N'_a(s)m - N_a(s)(\mathbf{W}\boldsymbol{\varphi}').\mathbf{n}\right\}ds \tag{23}$$

The equation of motion can also be written in matrix notation as:

$$\mathbf{M}\ddot{\mathbf{u}}(t) + \mathbf{F}_{\text{int}}(\mathbf{u}(\mathbf{t})) = \mathbf{F}_{\text{ext}} \tag{24}$$

where $\mathbf{u(t)}$ are nodal displacements and rotations and $\ddot{\mathbf{u}}(\mathbf{t})$ are nodal accelerations. They are, respectively, defined

$$\mathbf{u(t)} = \begin{Bmatrix} \boldsymbol{\varphi}_1(t) \\ \psi_1(t) \\ \boldsymbol{\varphi}_2(t) \\ \psi_2(t) \\ \vdots \\ \boldsymbol{\varphi}_b(t) \\ \psi_b(t) \\ \vdots \\ \boldsymbol{\varphi}_n(t) \\ \psi_n(t) \end{Bmatrix}, \quad \ddot{\mathbf{u}}(\mathbf{t}) = \begin{Bmatrix} \ddot{\boldsymbol{\varphi}}_1(t) \\ \ddot{\psi}_1(t) \\ \ddot{\boldsymbol{\varphi}}_2(t) \\ \ddot{\psi}_2(t) \\ \vdots \\ \ddot{\boldsymbol{\varphi}}_b(t) \\ \psi_b(t) \\ \vdots \\ \ddot{\boldsymbol{\varphi}}_n(t) \\ \ddot{\psi}_n(t) \end{Bmatrix} \quad \text{with} \quad n = N_{\text{el}}(n_{\text{en}} - 1) + 1$$

as:

The dynamic response in post-buckling regime, will consider vibrations around the equilibrium point (Meek & Xue, 1996). In order to recover the corresponding static solution response with dynamic analysis, it is necessary to introduce a damping to avoid this vibration. In this work, we use the Rayleigh model (Armentani et al., 2006). The damping matrix is defined proportional to the stiffness and mass matrix as:

$$\mathbf{C} = \alpha_1 \mathbf{K} + \beta_1 \mathbf{M} \tag{25}$$

where $\mathbf{K}, \mathbf{M}$ are the stiffness and mass matrix, respectively, α_1 and β_1 are constant to be defined from two given damping ratios that correspond to two selected vibration frequencies. The use of relatively high damping leads to shorter vibration time to recovering the corresponding static response. The ideal choice would be to use a damping just a little bit higher than the critical damping of the system in the frequency band of loading excitation. Thus, the choice of α_1 and β_1 is the most important to get the suitable behaviour.
If ω_i is a natural angular frequency of ith mode the both parameters must satisfy the relation:

$$\xi_i = \frac{\alpha_1}{2\omega_i} + \frac{\beta_1 \omega_i}{2} \tag{26}$$

where ξ_i is a damping factor, is defined as the ratio between the effective and the critical damping.

By considering this last equation and assuming that the damping factor ξ is approximately constant for defined band frequencies between ω_i and ω_j, we obtain a system of two equations, where α_1 and β_1 are unknowns. Solving this system we get:

$$\begin{aligned} \alpha_1 &= \frac{2\xi\omega_i\omega_j}{\omega_i+\omega_j} \\ \beta_1 &= \frac{2\xi}{\omega_i+\omega_j} \end{aligned} \tag{27}$$

This proportional coefficient damping can be determined using experimental modal testing combined with analysis method. The forced vibration experimental response can be given in the form of set of frequency response function (FRF'S). The frequency and damping are estimated from one or more FRFs by curve fitting them using an analytical model that includes frequency and damping as unknown parameters. This experimental method is based on performing some FRF measurements of the structure.

In the frequency band of FRF measurement, the frequency and damping for all modes are obtained by setting the experimental modal analysis. These experimental frequency and damping estimates can then be used to calculate the proportional damping matrix coefficients (see Schwarz et al., 2013)

This model has been proposed for linear behaviour. However, our problem is non-linear. It's interesting in this work to consider a non-linear damping as:

$$\mathbf{C} = \alpha_1 \mathbf{K_t} + \beta_1 \mathbf{M} \tag{28}$$

where $\mathbf{K_t}$ is the tangent matrix actualised each iteration in the Newton iterative procedure used for solving non-linear equations. The $\mathbf{K_t}$ is composed of geometric and material part like:

$$\mathbf{K_t} = \mathbf{K}_m + \mathbf{K}_g \tag{29}$$

We can use $\mathbf{K}_m$ or $\mathbf{K}_g$, or both of them to define the damping matrix. It will be illustrated later by example that the use of material part in damping matrix is the good choice.

If the damping is considered, the modified dynamic motion equations become:

$$\mathbf{M\ddot{u}(t)} + \mathbf{C\dot{u}(t)} + \mathbf{F}_{\text{int}}\mathbf{(u(t))} = \mathbf{F}_{\text{ext}} \tag{30}$$

where $\dot{\mathbf{u}}(\mathbf{t})$ are the nodal velocities.

2.2. Integration scheme (Newmark scheme)

In this section, we present the Newmark scheme (Newmark, 1959). We consider that the nodal displacements and rotations, velocities and accelerations are known

at t_n and we would get their values at t_{n+1}. The equilibrium equation is written at $t_{n+1} = t_n + h$ (h is the time step) as:

$$\mathbf{M}\ddot{\mathbf{u}}_{n+1} + \mathbf{C}\dot{\mathbf{u}}_{n+1} + \mathbf{F}^{\text{int}}_{n+1} = \mathbf{F}^{\text{ext}}_{n+1} \tag{31}$$

For computing the complete solution at time t_{n+1}, including the velocities and the accelerations, the Equation (31) should be supplemented with the standard Newmark equations defining the corresponding approximations for acceleration and velocity:

$$\ddot{\mathbf{u}}_{n+1} = \frac{1}{\beta h^2}\left\{\mathbf{u}_{n+1} - \mathbf{u}_n\right\} + \frac{-1}{\beta h}\dot{\mathbf{u}}_n + \left(1 - \frac{1}{2\beta}\right)\ddot{\mathbf{u}}_n \tag{32}$$

$$\dot{\mathbf{u}}_{n+1} = \frac{\gamma}{\beta h}\left\{\mathbf{u}_{n+1} - \mathbf{u}_n\right\} + \left(1 - \frac{\gamma}{\beta}\right)\dot{\mathbf{u}}_n + \left(1 - \frac{\gamma}{2\beta}\right)\ddot{\mathbf{u}}_n h \tag{33}$$

We can rewrite these equations as:

$$\ddot{\mathbf{u}}_{n+1} = \frac{1}{\beta h^2}\left\{\mathbf{u}_{n+1} - \mathbf{u}_n\right\} + \ddot{\mathbf{u}}^0_{n+1} \tag{34}$$

$$\dot{\mathbf{u}}_{n+1} = \frac{\gamma}{\beta h}\left\{\mathbf{u}_{n+1} - \mathbf{u}_n\right\} + \dot{\mathbf{u}}^0_{n+1} \tag{35}$$

where,

$$\ddot{\mathbf{u}}^0_{n+1} = \frac{-1}{\beta h}\dot{\mathbf{u}}_n + \left(1 - \frac{1}{2\beta}\right)\ddot{\mathbf{u}}_n \tag{36}$$

$$\dot{\mathbf{u}}^0_{n+1} = \left(1 - \frac{\gamma}{\beta}\right)\dot{\mathbf{u}}_n + \left(1 - \frac{\gamma}{2\beta}\right)\ddot{\mathbf{u}}_n h \tag{37}$$

The substitution of (34) and (35) into (31) leads to a set of non-linear equations, where the unknown values are the displacements and rotation at timet_{n+1}:

$$\frac{1}{\beta h^2}\mathbf{M}\left\{\mathbf{u}_{n+1} - \mathbf{u}_n\right\} + \frac{\gamma}{\beta h}\mathbf{C}\left\{\mathbf{u}_{n+1} - \mathbf{u}_n\right\} + \mathbf{F}^{\text{int}}_{n+1}(\mathbf{u}_{n+1}) = \mathbf{F}^{\text{ext}}_{n+1} - \ddot{M}\mathbf{u}^0_{n+1} - \dot{C}\mathbf{u}^0_{n+1} \tag{38}$$

Table 1. Computational procedure of Newmark scheme with an iterative procedure.

(1) Initialisation of displacement and rotation in each time step in the beginning of iteration procedure:

$\mathrm{u}^0_{n+1} = \mathrm{u}_n$

(2) Compute the velocity and acceleration at iteration 0

$\ddot{\mathrm{u}}^0_{n+1} = \frac{-1}{\beta h}\dot{\mathrm{u}}_n + (1 - \frac{1}{2\beta})\ddot{\mathrm{u}}_n$

$\dot{\mathrm{u}}^0_{n+1} = (1 - \frac{\gamma}{\beta})\dot{\mathrm{u}}_n + (1 - \frac{\gamma}{2\beta})\ddot{\mathrm{u}}_n h$

(3) At each iteration i we compute the incremental displacement and rotation, solving:

$\left(\frac{1}{\beta h^2}\mathrm{M} + \frac{\gamma}{\beta h}\mathrm{C}^{i-1} + \mathrm{K}_T^{i-1}(\mathrm{u}^{i-1}_{n+1})\right)\Delta\mathrm{u}^i_{n+1} = \mathrm{F}^{\mathrm{ext}}_{n+1} - \mathrm{F}^{\mathrm{int}}_{n+1}(\mathrm{u}^{i-1}_{n+1}) - \mathrm{M}\ddot{\mathrm{u}}^{i-1}_{n+1} - \mathrm{C}^{i-1}\dot{\mathrm{u}}^{i-1}_{n+1}$

(4) The correction of displacement, rotation and velocity and acceleration at each iteration until the convergence.

$\mathrm{u}^i_{n+1} = \mathrm{u}^{i-1}_{n+1} + \Delta\mathrm{u}^i_{n+1}$

$\ddot{\mathrm{u}}^i_{n+1} = \frac{1}{\beta h^2}\Delta\mathrm{u}^i_{n+1} + \ddot{\mathrm{u}}^{i-1}_{n+1}$

$\dot{\mathrm{u}}^i_{n+1} = \frac{\gamma}{\beta h}\Delta\mathrm{u}^i_{n+1} + \dot{\mathrm{u}}^{i-1}_{n+1}$

It can be written as:

$$\mathbf{R}(\mathbf{u}_{n+1})\frac{1}{\beta h^2}\mathbf{M}\{\mathbf{u}_{n+1} - \mathbf{u}_n\} + \frac{\gamma}{\beta h}\mathbf{C}\{\mathbf{u}_{n+1} - \mathbf{u}_n\} + \mathbf{F}^{\mathrm{int}}_{n+1}(\mathbf{u}_{n+1}) - \mathbf{F}^{\mathrm{ext}}_{n+1} + \mathbf{M}\ddot{\mathbf{u}}^0_{n+1} + \mathbf{C}\dot{\mathbf{u}}^0_{n+1} = 0 \tag{39}$$

If the Newton iterative method is used for that purpose, we may compute the linearised form of (39). This last can be computed using the Lie derivative formalism (see (Ibrahimbegović & Al Mikdad, 2000)). At typical iteration '*i*', the consistent linear approximation of (39) will take the following form:

$$L(\mathbf{R}(\mathbf{u}^i_{n+1})) = \mathbf{R}(\mathbf{u}^{i-1}_{n+1}) + \frac{\partial}{\partial\, \mathit{э}}\bigg|_{\mathit{э}=0}\left[\mathbf{R}_{\mathit{э}}(\mathbf{u}^{i-1}_{n+1} + \mathit{э}\ \Delta\mathbf{u}^i_{n+1})\right] \tag{40}$$

where

$$\mathbf{u}^i_{n+1} = \mathbf{u}^{i-1}_{n+1} + \mathit{э}\ \Delta\mathbf{u}^i_{n+1} \tag{41}$$

And $\Delta\mathbf{u}^i_{n+1}$ is the corresponding iterative update of incremental displacement and rotation. These are provided by solving the system below:

$$\left(\frac{1}{\beta h^2}\mathbf{M} + \frac{\gamma}{\beta h}\mathbf{C}^{i-1} + \mathbf{K}_T^{i-1}(\mathbf{u}^{i-1}_{n+1})\right)\Delta\mathbf{u}^i_{n+1} = \mathbf{F}^{\mathrm{ext}}_{n+1} - \mathbf{F}^{\mathrm{int}}_{n+1}(\mathbf{u}^{i-1}_{n+1}) - \ddot{M}\mathbf{u}^{i-1}_{n+1} - \mathbf{C}^{i-1}\dot{\mathbf{u}}^{i-1}_{n+1} \tag{42}$$

with

$$\mathbf{K}_T^{i-1}(\mathbf{u}^{i-1}_{n+1}) = \mathbf{R}(\mathbf{u}^{i-1}_{n+1}) + \frac{\partial}{\partial\, \mathit{э}}\bigg|_{\mathit{э}=0}\left[\mathbf{F}^{\mathrm{int}}_{n+1\mathit{э}}(\mathbf{u}^{i-1}_{n+1} + \mathit{э}\ \Delta\mathbf{u}^i_{n+1})\right] \tag{43}$$

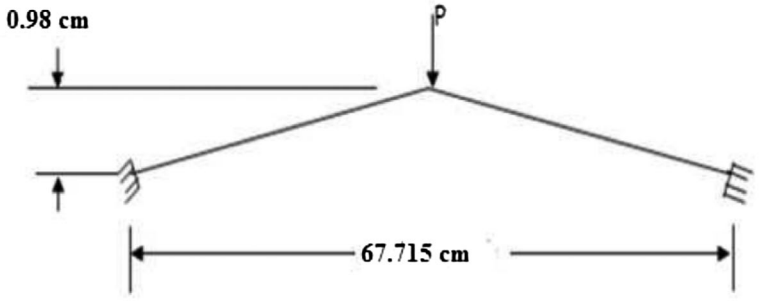

Figure 1. Geometry and load condition of toggle frame.

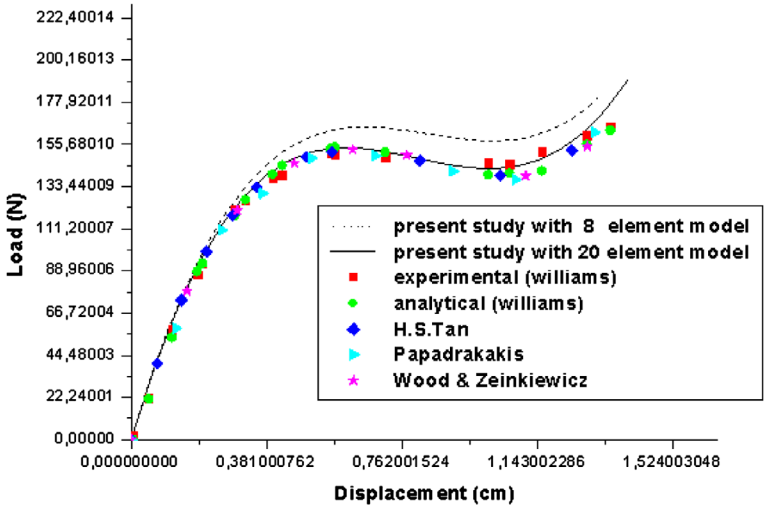

Figure 2. Load-displacement path of toggle frame, static analysis.

and

$$\mathbf{C}^{i-1} = \alpha_1 \mathbf{K}_T^{i-1} + \beta_1 \mathbf{M} \tag{44}$$

The velocity and acceleration must be updated at each iteration '*i*' using (34) and (35) as:

$$\ddot{\mathbf{u}}_{n+1}^{i} = \frac{1}{\beta h^2} \Delta \mathbf{u}_{n+1}^{i} + \ddot{\mathbf{u}}_{n+1}^{i-1} \tag{45}$$

$$\ddot{\mathbf{u}}_{n+1}^{i} = \frac{\gamma}{\beta h} \Delta \mathbf{u}_{n+1}^{i} + \dot{\mathbf{u}}_{n+1}^{i-1} \tag{46}$$

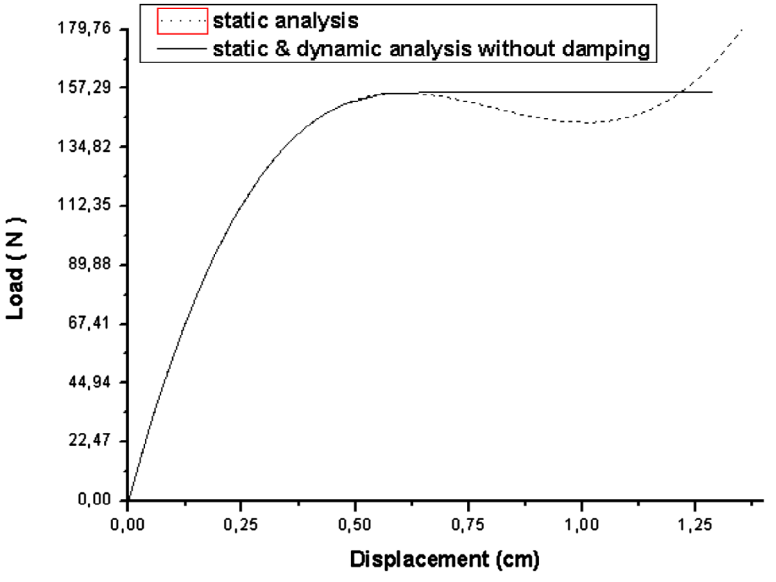

Figure 3. Load-displacement path of toggle frame, static and dynamic analysis with 20 elements model.

The computational procedure is summarised for typical time step in Table 1.

3. Numerical validation

In this section, we present some examples in order to illustrate the efficiency of the proposed approach for the post-buckling analysis. The computations are performed by FEAP (Finite Element Analysis Programme), developed by R. L. Taylor (Zienkiewicz & Taylor, 1991), at University of California, Berkley.

3.1. Williams toggle frame

The Williams toggle frame in Figure 1 is made up of two members with following properties: EI = $2.66.10^5$ N cm^2, EA = $8.251.10^6$ N, $\rho = 7.79.10^{-3}$ kg/cm^3.The frame is loaded by a concentrated force at the apex point connecting the two members. An analytical and experimental solution is presented by Williams in (Williams, 1964). A numerical solution is presented by Wood and Zeinkiewicz (1977), Papadrakakis (1981), Tan (1985) and Meek and Xue (1996, 1998).The frame has been modelled with 8 and 20 two nodes element model.

First, the static analysis has been performed using displacement control method or arc length method for tracing the load-deflection path. Figure 2 shows that our results are similar to the results obtained by Williams in (1964), Papadrakakis (1981), Tan (1985) and Wood and Zeinkiewicz (1977). The first limit point is

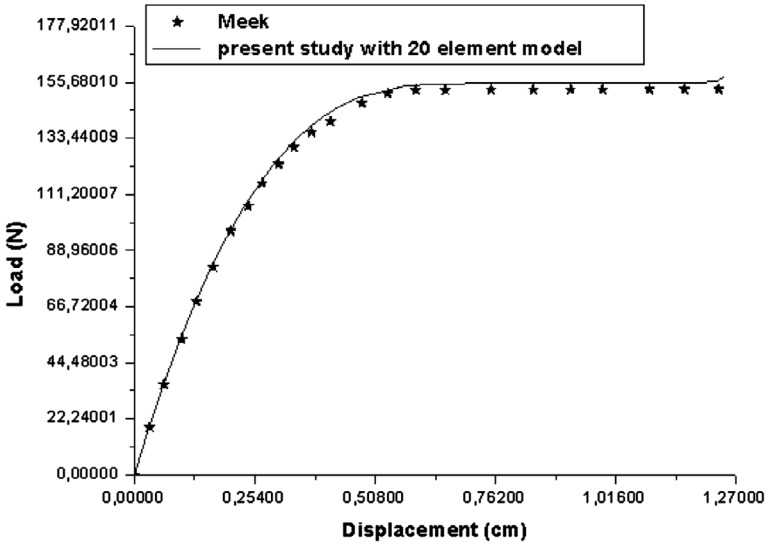

Figure 4. Load-displacement path of toggle frame, dynamic analysis.

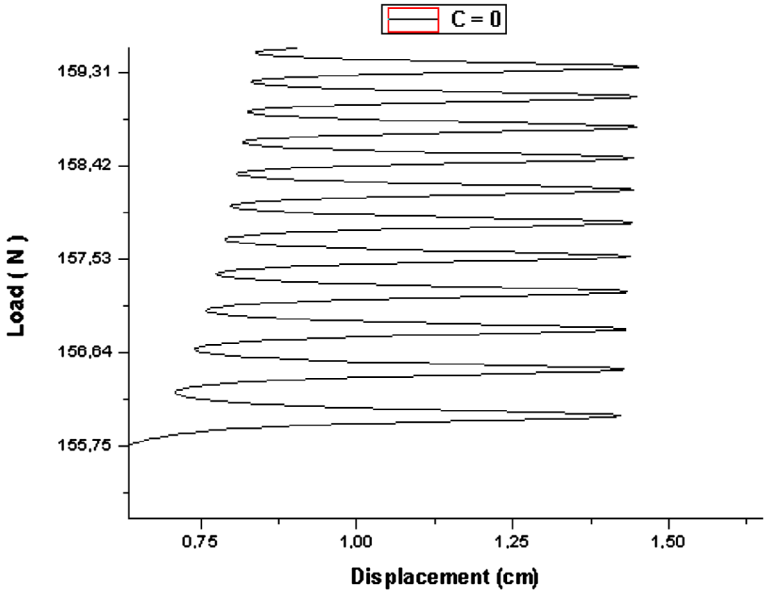

Figure 5. Load-displacement path of toggle frame around equilibrium point A (zoomed zone in Figure 3).

obtained at 164.58 lb with the model with 8 elements, and the second one with 20 elements is around 153.46 N (see Figure 2).

The second analysis has been performed using the static analysis with load control method before the limit point and the dynamic analysis with the Newmark

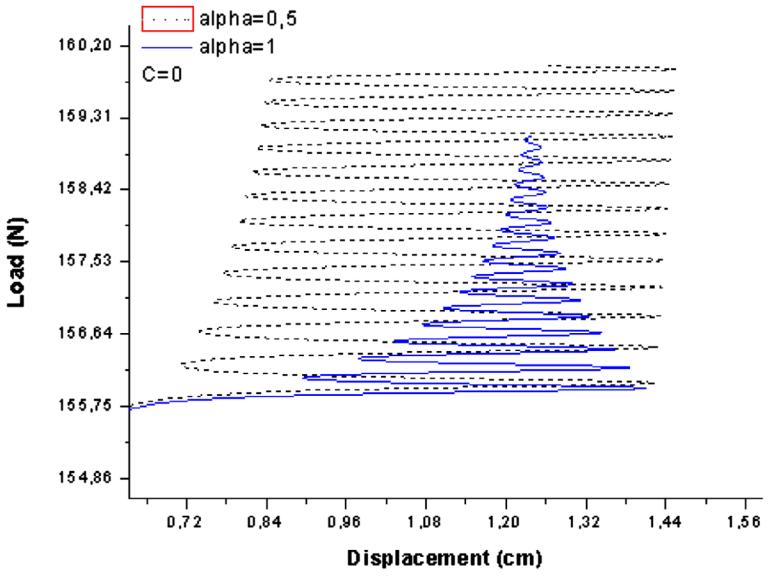

Figure 6. Load-displacement path of toggle frame, dynamic analysis using HHT-α scheme.

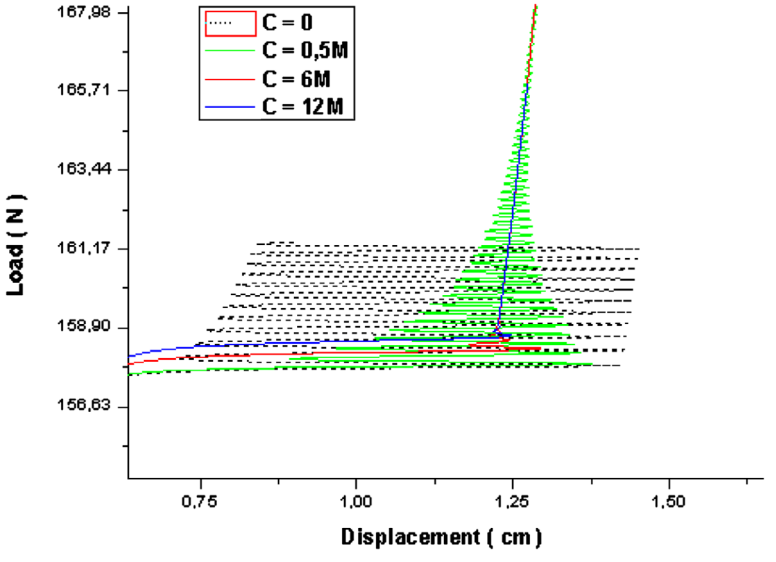

Figure 7. Load-displacement path of toggle frame around the equilibrium point A: using damping proportional to mass matrix.

scheme beyond the limit point. The last one analysis has been done with a time step for .1 s and a slow load increment rate for .0117 N/s.

Figure 3 shows that we can trace the load-deflection path after the limit point without down loading using dynamic analysis. Our results are similar to those presented by Meek and Xue (1996) (see Figure 4).

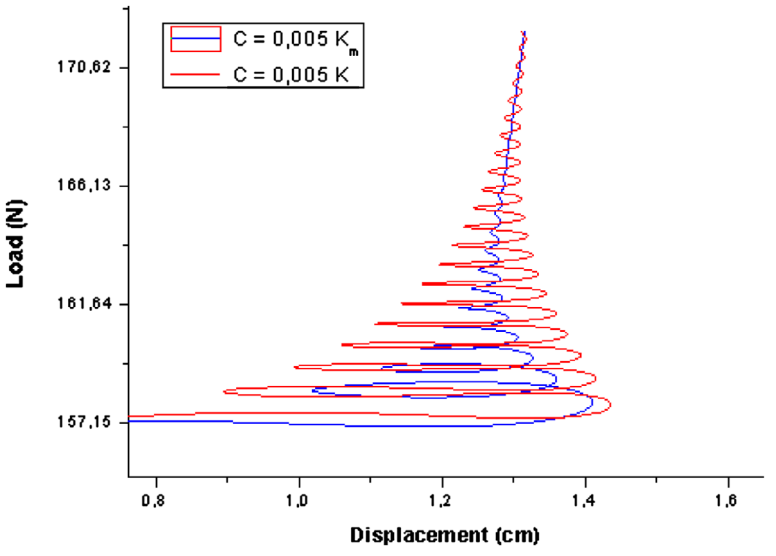

Figure 8. Load-displacement path of toggle frame around the equilibrium point A: using damping proportional to tangent matrix (total matrix & material part).

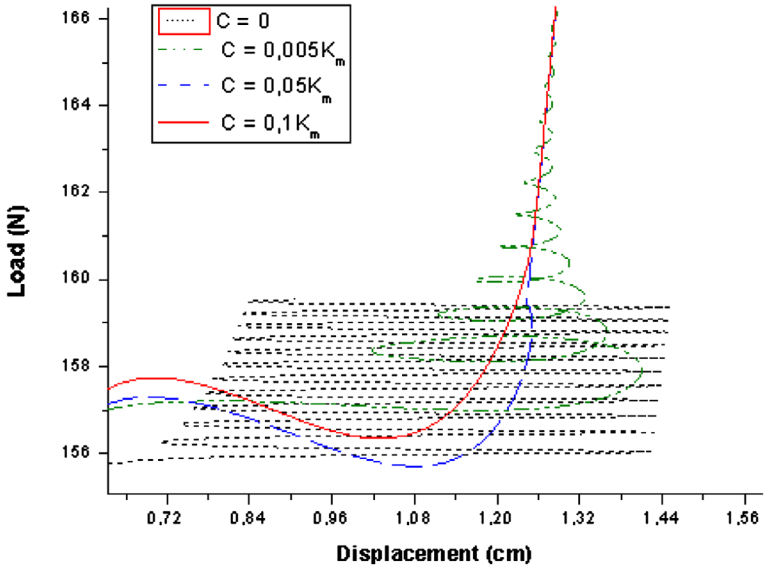

Figure 9. Load-displacement path of toggle frame around the equilibrium point A: using damping proportional to material part of tangent matrix.

Oscillations are observed around the equilibrium point A (see Figure 5). This behaviour can be improved using a dissipative scheme like HHT-alpha algorithm (see (Hilber et al., 1977)). For that purpose, we use HHT-α method for dynamic analysis with $\beta = .5$, $\gamma = 1$ and $.5 \leq \alpha \leq 1$.

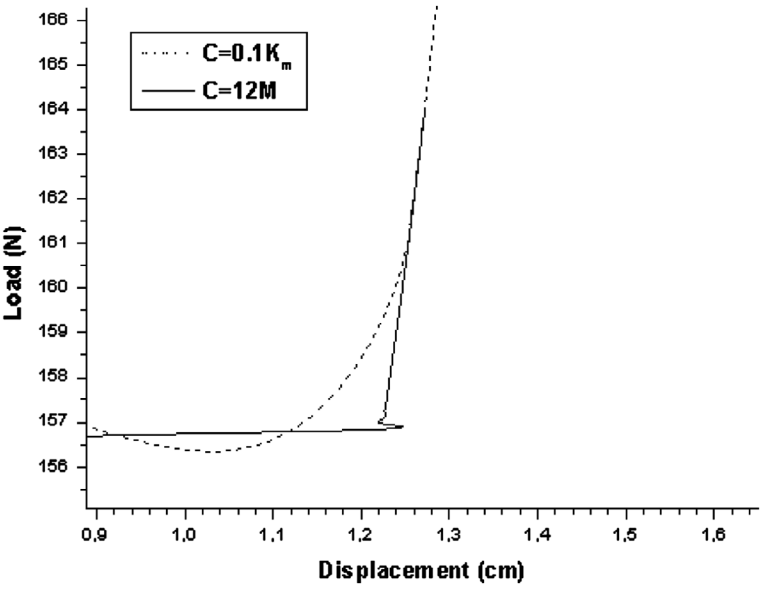

Figure 10. Load-displacement path of toggle frame around the equilibrium point A: comparison between two damping model effect.

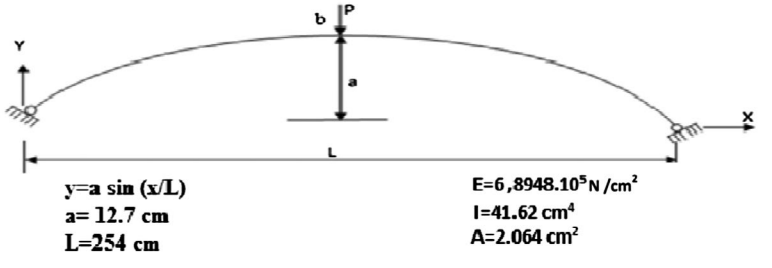

Figure 11. Geometry, material properties and load condition of shallow arch.

Figure 6 shows that the HHT-α integration scheme reduces the oscillation, but such reduction is not enough. So, the use of damping is necessary to follow full static analysis response.

To damp out this vibration around the equilibrium point, we use the Rayleigh damping model. Different damping coefficients were tested. First, damping matrix proportional only to the mass matrix with the three values of $\beta_1 = .5$, $\beta_1 = 6$ and $\beta_1 = 12$. In Figure 7, the response follows the static one after the equilibrium point A, but just the last value can be adopted.

In the second analysis as is mentioned before, we propose to use a non-linear damping by considering the tangent matrix. We start by considering a damping proportional to the complete tangent matrix, and we compare the behaviour when just the material tangent matrix is used. As it is illustrated in Figure 8, the use of material tangent matrix gives a better dissipation compared to the complete one.

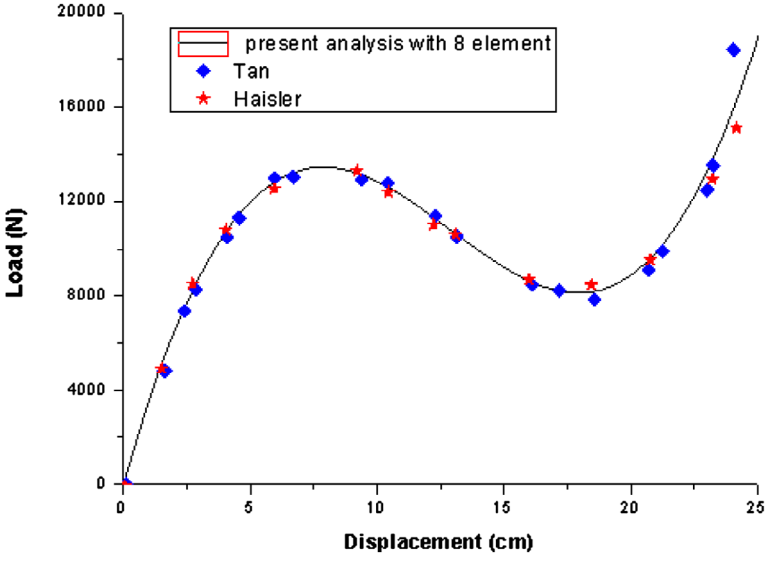

Figure 12. Load-displacement path of shallow arch, static analysis.

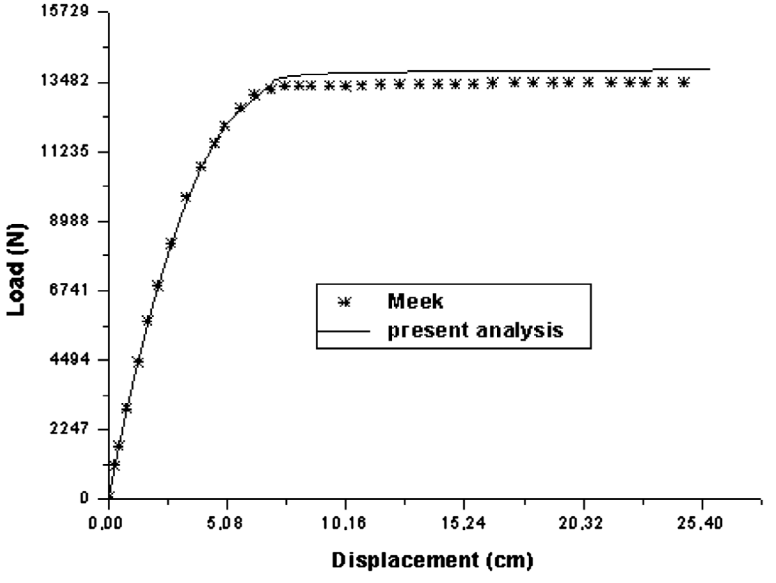

Figure 13. Load-displacement path of shallow arch, dynamic analysis.

Based on this last result, we have kept a damping only proportional to the material matrix part with different value of $\alpha_1 = .005$, $\alpha_1 = .05$ and $\alpha 1 = .1$. We are able to follow the static response without vibration (see Figure 9).

In conclusion, we can use a damping proportional to the matrix mass or material tangent matrix or the both to get the good behaviour around the equilibrium point (see Figure 10).

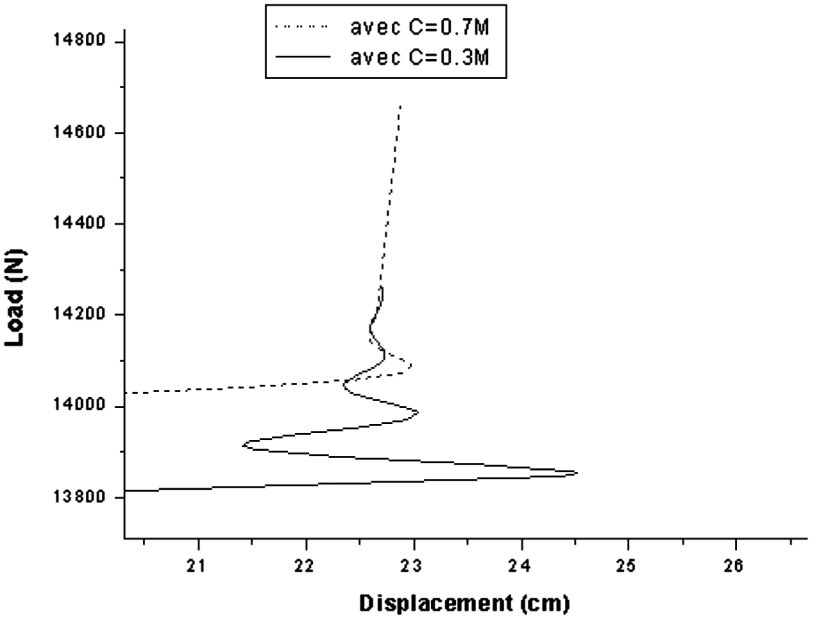

Figure 14. Load-displacement path of shallow arch, dynamic analysis around the equilibrium point A.

3.2. Shallow arch

A shallow arch with concentrated load acting at its apex is presented in Figure 11. The structure has the following material properties: EI = 28.69 10^7 N cm^2, EA = 14.23 10^6 N and ρ = 5.22 kg/cm^3. The geometrical description is shown in Figure 11.

An analytical solution has been presented by Timoshenko and Gere (1961), and a numerical solution is given by Haisler, Stricklin, and Key (1977) and Tan (1985) using different models. In this work, we have used eight elements of two nodes elements model. A static analysis has been done using the displacement control method for tracing the load-deflection path. The results obtained with the present approach are compared with computations by Tan (1985) and Haisler et al. (1977) (see Figure 12).

Before the limit point, the load-deflection path has been found using a static analysis with a displacement control method, and after this point, a dynamic analysis has been done with a time step for .1 s and slow rate of load .00448 N/s. The comparing between these two analyses proves that we can trace the load-deflection path without down loading.

Our results are similar to those obtained by Meek and Xue (1996) (see Figure 13). The observed difference is related to mass matrix, Meek and Xue (1996) neglects the inertial part or in this work is considered.

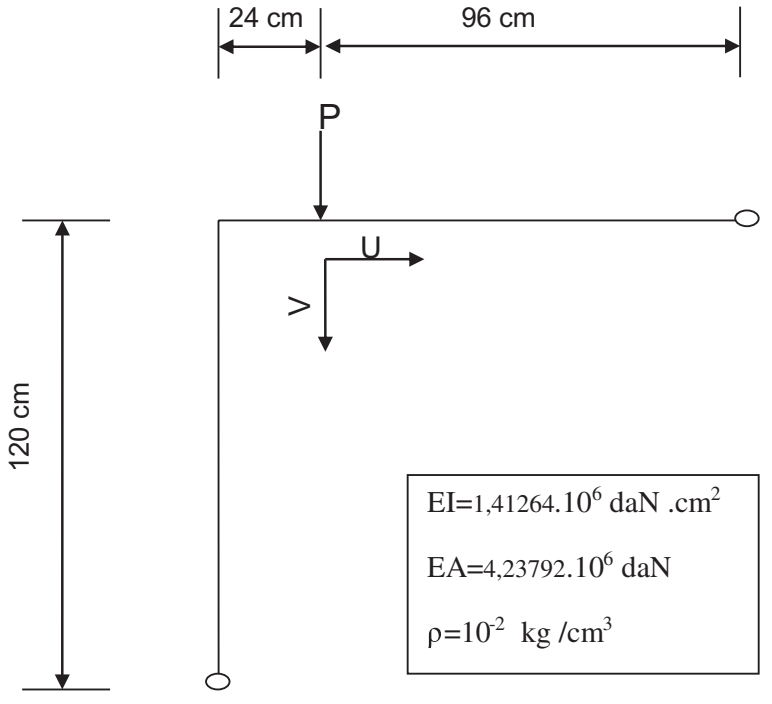

Figure 15. Geometry, material property and load condition of two bar frame.

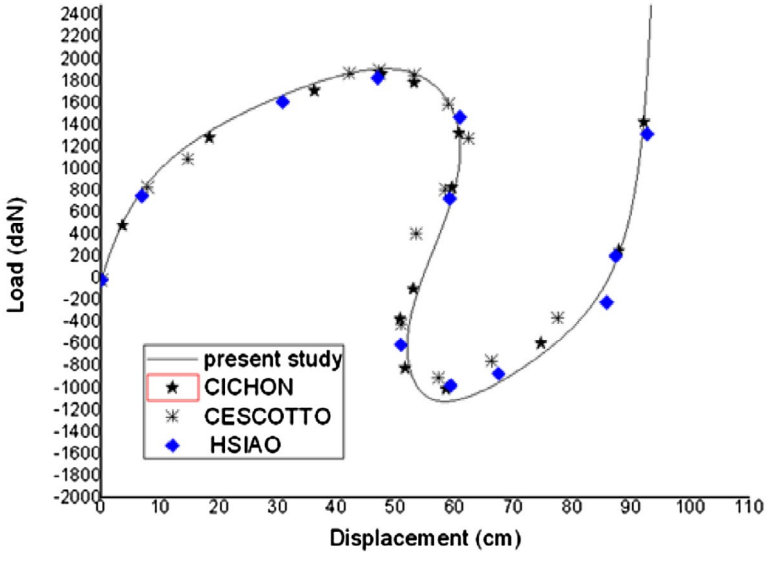

Figure 16. Two bar frame: static analysis, different studies.

The observed vibration around the equilibrium point is damped using the Rayleigh model proportional to mass matrix only. This choice $C = .7$ M is enough to follow the static solution (see Figure 14).

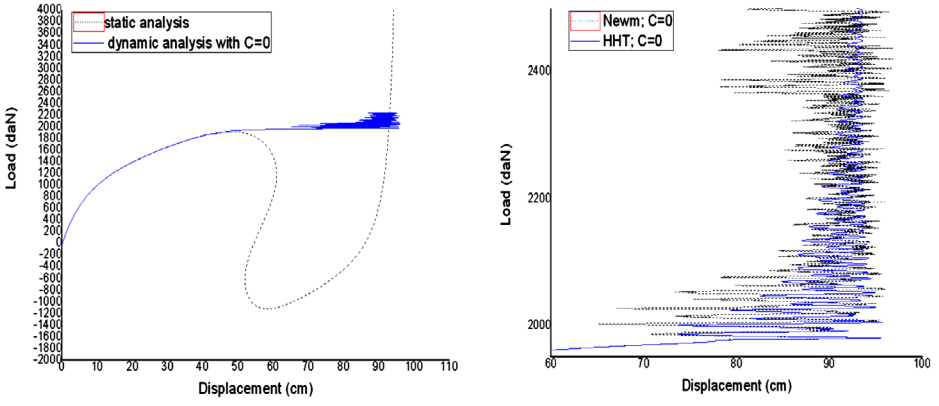

Figure 17. Two bar frame: Static and dynamic analysis, Newmark & HHT-α scheme, without damping.

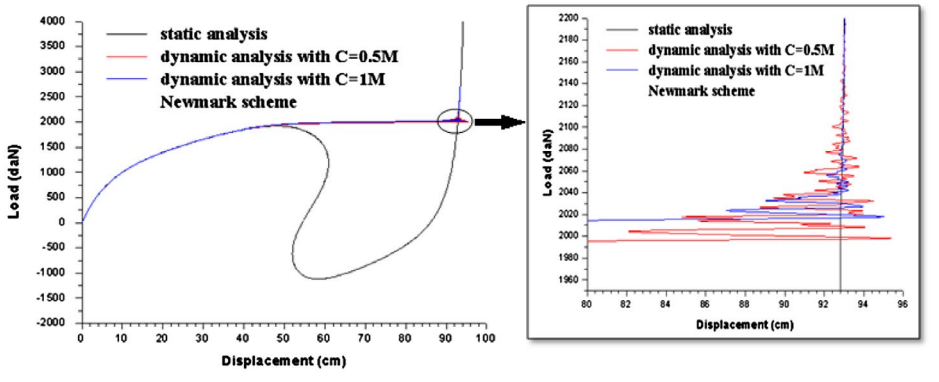

Figure 18. Two bar frame: Static and dynamic analysis, Newmark scheme, damping $C = .5$ M & $C = 1$ M.

3.3. Two bar frame

This example is used to illustrate the snap-back behaviour, is made up of two identical members which their properties are: EI = 1,41,264.10^6 daN.cm^2, EA = 4.23792.10^6 daN, $\rho = 10^{-2}$ kg /cm^3 (see Figure 15). The frame is loaded by a concentrated force on the horizontal bar with eccentricity of 24 cm from the joint of these two members.

The frame has been modelled with 10 elements.

The displacement control method adopted in the precedent examples for tracing a static load-deflection path, cannot be used for the snap-back behaviour (see Figure 16). The arc length method is adopted. The results are compared with Cescotto (1977), Cichon (1984) and Kuo Mo Hsiao (1987) (see Figure 16).

Using dynamic analysis, with time step for .01 s and a slow load increment rate for .005 daN/s, we can trace load-deflection path without down loading as is shown in Figure 17.

The observed vibrations around equilibrium point Figure 17, are damped with Rayleigh damping model: $\mathbf{C} = \beta_1 \mathbf{M}$. (see Figure 18).

Finally, these vibrations converge to the stable solution obtained with static analysis.

4. Conclusion

In this work, we have explored the post-buckling analysis by using a dynamic relaxation approach. This approach presents an advantage compared to static analysis in that it allows the finding of the equilibrium point after the limit point, without decreasing loading. Thus, there is no need to dedicated solution procedures; which can handle non-linear instability, snap-through or snap-back problems only by decreasing the loading in the post-buckling regime.

We have chosen the implicit scheme of Newmark integration for solving non-linear dynamic problem combined with Newton's method. The use of a dissipation scheme like HHT-α method can improve and reduce the vibration around the equilibrium point.

We have demonstrated through examples that when we use this approach, we are able to trace the load-displacement path without downloading after limit point using the slow rate of load increment. Vibration is observed around the equilibrium point in the presence of inertia force, it is necessary to consider damping. The Rayleigh damping model proportional to mass matrix or material tangent matrix is considered in this work. As conclusion, this approach converges to the same solution obtained with non-linear static analysis, but in the manner that is closer to a more realistic post-buckling behaviour of structure.

Disclosure statement

No potential conflict of interest was reported by the authors.

ORCID


Adnan Ibrahimbegovic http://orcid.org/0000-0002-6502-0198

References

Armentani E, Cali C, Cricrí G, Caputoc F, & Esposito, R. (2006). Numerical solution techniques for structural instability problems. *Journal of Achievements in Materials and Manufacturing Engineering, 19*, 53–64.

Bathe, K. J., & Noh, G. (2012). Insight into an implicit time integration scheme for structural dynamics. *Computers & Structures, 98–99*, 1–6.

Bathe, K. J., Ramm, E., & Wilson, E. L. (1976). Finite element formulations for large deformation dynamic analysis. *International Journal for Numerical Methods in Engineering, 9*, 353–386.

Belytschko, T., & Hsieh, B. J. (1973). Non-linear transient finite element analysis with convected co-ordinates. *International Journal for Numerical Methods in Engineering, 7*, 255–271.

Cescotto S. (1977). Study of large displacement and high strain by finite element method (Phd thesis). Belgium: LIEGE.

Chung, J., & Hulbert, G. (1993). A time integration algorithm for structural dynamics with improved numerical dissipation: The generalized-α method. *Journal of Applied Mechanics, 60*, 371–375.

Cichoń, C. (1984). Large displacements in-plane analysis of elastic-plastic frames. *Computers & Structures, 5*, 737–745.

Crisfield M. A. (1991).*Nonlinear finite element analysis of solids and structures*. Vol. 1. Chichester: Jonh Wiley Chichester.

Haisler, W. E., Stricklin, J. H., & Key, J. E. (1977). Displacement incrementation in non-linear structural analysis by the self-correcting method. *International Journal for Numerical Methods in Engineering, 11*, 3–10.

Hilber, H. M., Hughes, T. J. R., & Taylor, R. L. (1977). Improved numerical dissipation for time integration algorithms in structural dynamics. *Earthquake Engineering & Structural Dynamics, 5*, 282–292.

Ibrahimbegović, A. (1995). On finite element implementation of geometrically nonlinear Reissner's beam theory: Three-dimensional curved beam elements. *Computer Methods in Applied Mechanics and Engineering, 122*, 11–26.

Ibrahimbegović, A., Al Mikdad, M. (2000). Quadratically convergent direct calculation of critical points for 3d structures undergoing finite rotations. *Computer Methods in Applied Mechanics and Engineering, 189*, 107–120.

Ibrahimbegovic A. (2009). *Nonlinear solid mechanics: Theoretical formulations and finite element solution methods*. New York, NY: Springer.

Ibrahimbegović, A., & Frey, F. (1993). Finite element analysis of linear and non-linear planar deformations of elastic initially curved beams. *International Journal for Numerical Methods in Engineering, 36*, 3239–3258.

Ibrahimbegovic, A., Knopf-Lenoir, C., Kucerova, A., & Villon P. (2004). Optimal design and optimal control of structures undergoing finite rotations and elastic deformations. *International Journal for Numerical Methods in Engineering, 61*, 2428–2460.

Ibrahimbegović, A., & Mamouri, S. (1999). Nonlinear dynamics of flexible beams in planar motion: Formulation and time-stepping scheme for stiff problems. *Computers & Structures, 70*, 1–22.

Ibrahimbegovic, A., & Mamouri, S. (2002). Energy conserving/decaying implicit time-stepping scheme for nonlinear dynamics of three-dimensional beams undergoing finite rotations. *Computer Methods in Applied Mechanics and Engineering, 191*, 4241–4258.

Ibrahimbegović, A., Shakourzadeh, H., Batoz, J. L., AI Mikdad M, & Guo Y. Q. (1996). On the role of geometrically exact and second-order theories in buckling and post-buckling analysis of three-dimensional beam structures. *Computers & Structures, 61*, 1101–1114.

Kuo Mo Hsiao, K. M. (1987). Nonlinear finite element analysis of elastic frames. *Computers & Structures, 26*, 693–701.

Mamouri S, & Ibrahimbegovic A. (2001). Modified HHT dissipation scheme for beams undergoing finite rotations. *European Journal of Computational Mechanics, 11*, 121–143.

Marsden, J. E., & Hughes, T. J. R. (1983). *Mathematical foundation of elasticity*. New York, NY: Dover Publications.

Meek, J. L., & Xue, Q.. (1996). A study on the instability problem for 2D-frames. *Computer Methods in Applied Mechanics and Engineering, 136*, 347–361.

Meek, J. L., & Qiang Xue (1998). A study on the instability problem for 3D-frames. *Computer Methods in Applied Mechanics and Engineering, 158*, 235–254.

Newmark, N. M. (1959). A method of computational for structural dynamics. *Journal of Engineering Mechanics Division ASCE, 85*, 67–94.

Papadrakakis, M. (1981). Post-buckling analysis of spatial structures by vector iteration methods. *Computers & Structures, 14*, 393–402.

Schwarz B., & Richardson M. (2013). *Proportional Damping from Experimental Data*. Proceedings of the 31st IMAC, a conference on structural dynamics, Conference Proceedings of the Society for Experimental Mechanics Series 45, Topics in Modal Analysis, Volume 7, Chapter 17, R. Allemang et al. (eds.).

Tan H. S. (1985). Finite element analysis of the elastic, non-linear response of frames, plates and arbitrary shells to static loads (Phd thesis). Brisbane: University of Queensland.

Timoshenko, S., & Gere, J. M. (1961). *Theory of elastic stability* (2nd ed.). New York, NY: McGraw Hill.

Williams, F. W. (1964). An approach to the non-linear behaviour of the members of a rigid jointed plane framework with finite deflections. *Quarterly Journal of Mechanics and Applied Mathematics, 17*, 456–469.

Wood R. D., & Zeinkiewisz O. C. (1977). Geometrically nonlinear finite element analysis of beams, frames, arches and axisymmetric shells. *Computers & Structures, 7*,725–735.

Zienkiewicz O. C., & Taylor R. L. (1991). Solid and fluid mechanics, dynamics and nonlinearity. London: Mc Graw-Hill.